IEEE Open Journal of Vehicular Technology

Received 8 November 2022; accepted 25 November 2022. Date of publication 2 December 2022;
date of current version 14 December 2022. The review of this article was coordinated by Editor B. Soret.

Digital Object Identifier 10.1109/OJVT.2022.3226192

Throughput Enhancement of Dynamic Full-Duplex Cellular System by Distributing Base Station Reception Function

KEITA FUKUSHIMA [1] (Student Member, IEEE), SHOTA MORI [1,2] (Student Member, IEEE), KEIICHI MIZUTANI [1] (Member, IEEE), AND HIROSHI HARADA [1] (Member, IEEE)

[1]Graduate School of Informatics, Kyoto University, Kyoto 606-8501, Japan
[2]School of Platforms, Kyoto University, Kyoto 606-8501, Japan

CORRESPONDING AUTHOR: HIROSHI HARADA (e-mail: hiroshi.harada@i.kyoto-u.ac.jp)

This article was presented in part to the 2022 IEEE 95th Vehicular Technology Conference (VTC2022-Spring), Helsinki, Finland, Jun. 2022 [1]. This work was supported by the Ministry of Internal Affairs and Communications in Japan under Grant JPJ000254.

ABSTRACT In-band full-duplex (IBFD) is a promising technology for improving spectral efficiency beyond 5G and 6G. The dynamic duplex cellular (DDC) system has been proposed as a method for the phased introduction of IBFD into cellular systems while maintaining backward compatibility. Although previous studies have shown that DDC systems can improve the average user throughput, twice the spectral efficiency compared to half-duplex (HD), ideally expected for IBFD, has not been achieved. The main component that disturbs throughput enhancement is the residual component of self-interference (SI) at the base station (BS), which SI cancellers cannot entirely suppress. In this study, we propose a DDC system with a dedicated transmitter (DT) and multiple distributed receivers called remote receivers (RRs) for the BS to reduce the effective SI and enhance uplink reception quality. We implement user equipment scheduling and power control for the DDC system in the topology with DT and multiple RRs and improvement by IBFD. evaluate its performance using computer simulations in a single-cell environment. The proposed DDC system with receiver-distributed topology achieves up to 96% improvement in average user throughput of uplink and downlink from the HD system with the same topology, which is close to the ideal performance.

INDEX TERMS Distributed BSs, dynamic duplex cellular, in-band full-duplex, local 5G, self-interference.

I. INTRODUCTION

Over the past few decades, mobile data traffic has increased rapidly [2]. By 2023, 71% of the world's population (5.7 billion people) are expected to use mobile connectivity services, and the number of smartphone subscriptions is expected to increase by 7% annually [3]. In addition, the number of machine-to-machine (M2M) terminals supporting the Internet of Things (IoT) platforms has increased significantly and is expected to grow by 30% annually [3]. To meet these demands, the 5th generation mobile communication system (5G) implements new technologies, such as massive multiple-input multiple-output (MIMO) technology using many antenna elements, allocation of new high-frequency bands, such as the 28 GHz band, and 5G new radio (5G NR)—a flexible frame composition technology that can meet wide bandwidth and low latency requirements [4], [5], [6]. However, to cope with the ever-growing traffic requirements, the conventional spectrum below 6 GHz (i.e., the sub-6 GHz band) must also be used more efficiently. This requires introducing new technologies that improve spectral efficiency beyond 5G and 6G [7], [8], [9], [10], [11], [12], [13].

In-band full-duplex (IBFD) is a promising technology for improving spectral efficiency beyond 5G and 6G [7], [8]. IBFD is a technique for operating uplink (UL) and downlink (DL) communications simultaneously in the same band, which doubles the spectral efficiency compared to half-duplex (HD) under ideal conditions [14], [15], [16], [17], [18]. Because IBFD allows simultaneous transmission and reception, the transmitted signal interferes with its own received signal, which is called the self-interference (SI) problem.

The cancellation of the SI is essential to ensure reception quality. Various methods have been proposed for antenna, analog, and digital domains [15], [16], [17], [18], [19], [20], [21], [22], [23]. However, SI cancellers are currently difficult to implement in mobile terminals, such as user equipment (UE) in cellular systems, because of their large implementation scale. User-paired IBFD (UP-IBFD), which performs IBFD only at the base station (BS) and allocates UL and DL communications to two different UEs, is considered relatively practical because the SI canceller is installed only at the BS [15]. Hereafter, the UP-IBFD is referred to as IBFD.

When applying the IBFD to cellular systems, it is important to maintain backward compatibility. If a legacy 5G system is suddenly replaced by a new cellular system based on IBFD, legacy 5G UEs become unavailable. Therefore, the dynamic duplex cellular (DDC) system has been proposed as a method for the phased introduction of IBFD into cellular systems [24], [25], [26]. The DDC system assumes the operation of the legacy 5G system and applies IBFD only when the interference to the communication of the legacy 5G system is sufficiently small by a scheduling scheme that includes the selection of a UE that can perform IBFD [24], [25], [26]. Although previous studies have shown that DDC systems can improve the average user throughput, twice the spectral efficiency compared to HD, which is ideally expected for IBFD, has not been achieved [24], [25], [26].

One of the factors limiting the improvement of spectral efficiency in DDC systems is the inter-user interference (IUI) caused by the UL-UE (UL communication-allocating UE) to the DL-UE (DL communication-allocating UE) when IBFD is applied. The impact of the IUI can be mitigated by appropriately selecting the pair of UEs to be assigned communication, and the IUI reduction method using successive interference cancellation has also been proposed [27]. The dominant factor limiting the improvement of the spectral efficiency in DDC systems is the residual component of the aforementioned SI, which cannot be fully suppressed by the SI canceller. Hereafter, the component is referred to as the residual SI. The current combination of SI cancellers can suppress SI by approximately 110 dB [15]. Although a 110 dB of SI cancellation performance is sufficient for considering the introduction of IBFD to wireless local area network (WLAN)-based systems [15], the residual SI component cannot be ignored in cellular systems because of the large transmission power of the BS.

To overcome this problematic large residual SI, techniques to suppress effective SI by separating and distributing the transmitting (Tx) and receiving (Rx) antennas of the BS have been proposed [28], [29]. The effective SI can be reduced by separating the Tx and Rx antennas and installing them at a distance apart. This concept of distributed placement of antennas is also common to the cell-free architecture, which is considered a promising candidate for next-generation cellular networks. Several studies have investigated various distributed antenna systems [30], [31], [32]. However, to the best of our knowledge, no previous study has proposed and evaluated a DDC system that incorporates the antenna distribution technique and includes a scheduling and power control scheme to mitigate interference and perform IBFD.

In this study, we propose a DDC system operating in the sub-6 GHz band with multiple distributed Rx-only antennas for the BS [1], including a scheduling scheme with UE selection and power control for the BS and UEs. In the proposed DDC system, the Tx and Rx antennas of the BS are separated. The Tx-only antenna of the BS of the proposed DDC system is installed at the location where the Tx/Rx antenna of the BS in the conventional DDC system is installed. In addition, multiple Rx-only antennas of the BS are distributed in a cell. These Tx-only and Rx-only antennas are connected to the signal processing and control unit of the BS (e.g., centralized unit (CU) and distributed unit (DU)) via a backbone network using radio-over-fiber (RoF) technology, similar to the radio unit (RU) of 5G or remote radio head (RRH) of 4G, to enable coordinated operation. Hereafter, the Tx-only and Rx-only antennas of the BS in the proposed DDC system are referred to as the *dedicated transmitter (DT)* and *remote receiver (RR)*, respectively. The proposed DDC system is expected to improve the UL communication quality when IBFD is applied because the path loss between DT and RRs mitigates the SI, and the UL communication path is shortened on average.

In our prior and shorter version of this study [1], we proposed the basic concept of the DDC system with a DT and multiple distributed RRs. Furthermore, we implemented UE scheduling and power control for the DDC system [24], [25], [26] in a topology with a DT and three RRs and evaluated its performance using link-level and system-level computer simulations. The present work further extends the above studies to design and evaluate the proposed system for the cases of distributed placements of one and six RRs. In addition, a new power control scheme for UL communications superimposed on DL communications is proposed and evaluated. These evaluations are performed in a single-cell environment, which is assumed to be a minimal configuration of local 5G [33], [34] and a hotspot-like deployment.

The main contributions of this study can be summarized as follows:

- A comprehensive proposal for a novel DDC system operating in the sub-6 GHz band that reduces SI by spatially separating transmission and reception functions through a distributed arrangement of receiving antennas is presented.
- Performance evaluation and comparison of the proposed DDC system and conventional DDC or existing HD systems using system-level simulations based on results of 5G link-level simulations are conducted.
- Compared to the existing HD system, the proposed DDC system can improve the average user throughput by more than 108% for UL and more than 95% for DL.

The remainder of this article is organized as follows: Section II introduces the basic operation of the DDC system using the conventional case where transmission and reception functions of the RU are not spatially separated [24], [25],

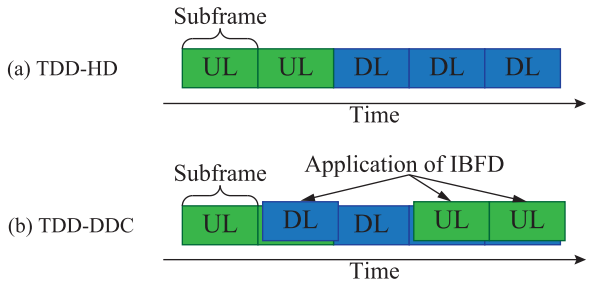

FIGURE 1. Duplex model.

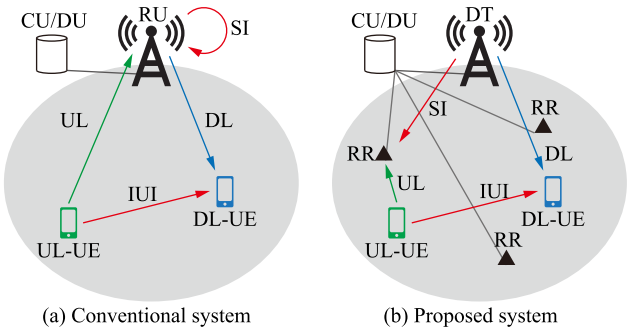

(a) Conventional system (b) Proposed system

FIGURE 2. Interference model.

[26]; Section III presents the proposed DDC system with a DT and distributed-multiple RRs; Section IV designs the optimal parameters of the proposed DDC system and evaluates its performance by using 5G-based link-level and system-level computer simulations; and Section V presents the conclusion of this study.

II. BASIC DESCRIPTION OF DDC SYSTEM

Here, the time-division duplex (TDD)-based conventional DDC systems [24], [25], [26], the basis of the proposed system, are described. First, we outline the basic principles of the DDC system. Next, an interference model for a conventional DDC system is presented. Finally, a scheduling scheme based on this interference model is described.

A. OUTLINE OF DDC SYSTEM PRINCIPLE

Fig. 1(a) shows the UL/DL switching schematic of a TDD-based HD system (TDD-HD). Although the UL/DL switching is possible on a symbol-by-symbol basis in the 5G [6], [35], in this study, we assumed switching on a subframe-by-subframe basis for simplicity. In Fig. 1(a), as an example, the first and second subframes are set to UL subframes (ULSFs) to be allocated to UL communications, and the third, fourth, and fifth subframes are set to DL subframes (DLSFs) to be allocated DL communications.

The TDD-based DDC system (TDD-DDC) allows the superimposition of DL communications with other UEs on the UL communications allocated in the ULSFs by applying IBFD, as shown in Fig. 1(b). Furthermore, it allows the superimposition of UL communications with other UEs on DL communications allocated to DLSFs. The IBFD applicable condition is that IUI does not degrade the DL communication quality in DLSF, and SI does not degrade the UL communication quality in ULSF. If these conditions are not satisfied, IBFD is not applied, and only HD communication is performed. For the UEs allowed to perform IBFD, an appropriate modulation and coding scheme (MCS) is selected according to the signal-to-interference and noise power ratio (SINR). To realize the DDC system, a scheduling scheme that includes UE selection is proposed.

B. INTERFERENCE MODEL

1) IBFD NON-APPLICABLE CASE

First, we describe the interference model when IBFD is not applied. Let us assume that there is one BS and N UEs in the cell. In the DLSF, a DL-UE, $d \in \mathscr{D}$, is determined by the scheduling method from the set of DL-UE candidates, $\mathscr{D} \subset \mathscr{N}$, where $\mathscr{N} = \{\varphi_0, \varphi_1, \ldots, \varphi_{N-1}\}$ is the set of all UEs in the cell, and φ_n represents the nth node in the cell. Thereafter, the SINR of DL communication from RU Ψ, to the DL-UE d, is expressed as follows:

$$\gamma_{d,\Psi}^{\mathrm{HD,DL}} = \frac{G_{\Psi,d} L_{d,\Psi} G_{d,\Psi} P_{\Psi}}{N_d B}, \tag{1}$$

where $G_{y,x}$ is the antenna gain from x to y, $L_{y,x}$ is the path loss between x and y, P_x is the Tx power of x, N_x is the noise power spectrum density at x, and B is the allocated bandwidth.

In ULSF, a UL-UE, $u \in \mathscr{U}$, is determined by the scheduling method from the set of UL-UE candidates, $\mathscr{U} \subset \mathscr{N}$. The SINR of UL communication from the UL-UE, u, to the RU, Ψ, is expressed as follows:

$$\gamma_{\Psi,u}^{\mathrm{HD,UL}} = \frac{G_{u,\Psi} L_{\Psi,u} G_{\Psi,u} P_u}{N_{\Psi} B}. \tag{2}$$

As shown in (1) and (2), when the IBFD is not applied, there is no interference because a single-cell environment is assumed in this study.

2) IBFD APPLICABLE CASE

Fig. 2(a) shows the intracell interference model when IBFD is applied to a conventional DDC system. When DL-UE, $d \in \mathscr{D}$, and UL-UE, $u \in \mathscr{U}$, are simultaneously allocated communications in the same subframe, the SINR of DL communication, $\gamma_{d,\Psi,u}^{\mathrm{FD,DL}}$, and the SINR of UL communication, $\gamma_{\Psi,u}^{\mathrm{FD,UL}}$, are, respectively, expressed as follows:

$$\gamma_{d,\Psi,u}^{\mathrm{FD,DL}} = \frac{G_{\Psi,d} L_{d,\Psi} G_{d,\Psi} P_{\Psi}}{N_d B + G_{u,d} L_{d,u} G_{d,u} P_u}, \tag{3}$$

$$\gamma_{\Psi,u}^{\mathrm{FD,UL}} = \frac{G_{u,\Psi} L_{\Psi,u} G_{\Psi,u} P_u}{N_{\Psi} B + C P_{\Psi}}, \tag{4}$$

where C is a coefficient representing the amount of SI cancellation at the BS that satisfies $0 \leq C \leq 1$.

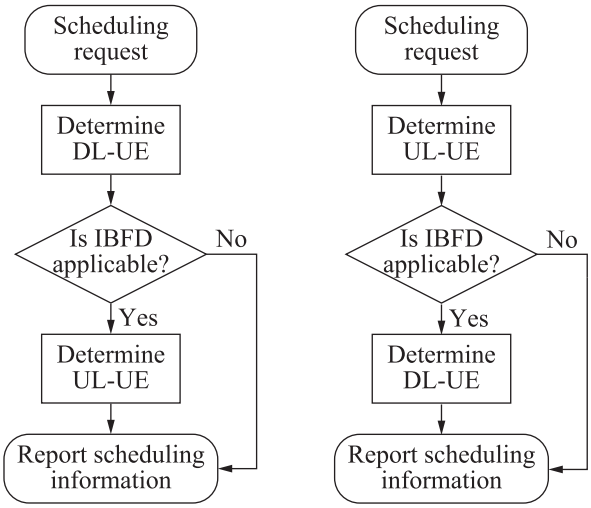

(a) DLSF (b) ULSF

FIGURE 3. Scheduling in the DDC system.

C. SCHEDULING

1) BASIC ALLOCATION METHOD

The basic allocation method in a DDC system is based on the proportional fairness scheduling (PFS) algorithm [36], which is widely used in 4G and 5G [37], [38]. In ULSF, the UL-UE to which the UL communication is allocated in nth transmission time interval (TTI), $u(n)$, is determined by the PFS algorithm as

$$u(n) = \arg\max_{\varphi_i \in \mathscr{U}} \frac{R_{\varphi_i}^{\mathrm{UL}}(n)}{\mathfrak{E}\left\{R_{\varphi_i}^{\mathrm{UL}}(n-1)\right\}}, \tag{5}$$

where $R_{\varphi_i}^{\mathrm{UL}}(n)$ is the instantaneous UL user throughput in nth TTI when the UL communication is allocated to φ_i, and $\mathfrak{E}\{R_{\varphi_i}^{\mathrm{UL}}(n-1)\}$ is the exponentially moving averaged UL user throughput of φ_i in $(n-1)$th TTI, which is updated for every TTI as follows:

$$\mathfrak{E}\left\{R_{\varphi_i}^{\mathrm{UL}}(n)\right\} = \left(1 - \frac{1}{T_{\mathrm{w}}}\right)\mathfrak{E}\left\{R_{\varphi_i}^{\mathrm{UL}}(n-1)\right\} + \frac{1}{T_{\mathrm{w}}} R_{\varphi_i}^{\mathrm{UL}}(n)\, p_{\varphi_i}^{\mathrm{UL}}(n), \tag{6}$$

where T_{w} is a coefficient representing the weight, and $p_{\varphi_i}^{\mathrm{UL}}(n)$ is a coefficient that is equal to 1 only if φ_i is allocated communication in nth TTI, and the allocated communication is successfully completed; otherwise, it is equal to 0. The determination of DL-UE, d, is represented in (5) and (6) by replacing $R_{\varphi_i}^{\mathrm{UL}}$, $\mathscr{U}$, and $p_{\varphi_i}^{\mathrm{UL}}$ with $R_{\varphi_i}^{\mathrm{DL}}$, $\mathscr{D}$, and $p_{\varphi_i}^{\mathrm{DL}}$, respectively. We assume that instantaneous throughput is calculated as a discrete value corresponding to the available MCS with the highest spectral efficiency.

2) DETERMINATION OF IBFD APPLICABILITY

Fig. 3 shows the scheduling flow of the DDC system. In the DLSF, DL-UE, $d \in \mathscr{D}$, is determined by the PFS algorithm using the SINR in HD, as shown in (1). Candidates for UL-UE, $u \in \mathscr{U}_d^{\mathrm{FD}}$, to be allocated superimposed UL communications, are selected. The set of candidates $\mathscr{U}_d^{\mathrm{FD}}$ can be expressed as

$$\mathscr{U}_d^{\mathrm{FD}} = \left\{\varphi_i \in \mathscr{U} \middle| R_d^{\mathrm{DL,HD}} = R_{d,\varphi_i}^{\mathrm{DL,FD}} \bigwedge R_{\varphi_i}^{\mathrm{UL,FD}} \neq 0\right\}, \tag{7}$$

where $R_d^{\mathrm{DL,HD}}$, $R_{d,\varphi_i}^{\mathrm{DL,FD}}$, and $R_{\varphi_i}^{\mathrm{UL,FD}}$ are the instantaneous user throughputs estimated using $\gamma_{d,\Psi}^{\mathrm{HD,DL}}$, $\gamma_{d,\Psi,\varphi_i}^{\mathrm{FD,DL}}$, and $\gamma_{\Psi,\varphi_i}^{\mathrm{FD,UL}}$, respectively. The conditions $R_d^{\mathrm{DL,\,HD}} = R_{d,\varphi_i}^{\mathrm{DL,FD}}$ in (7) indicate that there is no degradation in the existing DL communication. If $\mathscr{U}_d^{\mathrm{FD}} \neq \varnothing$, the UE to be allocated for the superimposed UL communication is determined by the PFS algorithm based on the SINR shown in (4). Otherwise, IBFD is not applied, and only DL communication is performed. These procedures for determining the applicability of IBFD and scheduling in DLSF are shown in Algorithm 1 as pseudo-code.

In ULSF, the UL-UE, $u \in \mathscr{U}$, is first determined by the PFS algorithm using the SINR in HD, as shown in (2). Second, the following conditions are checked to ensure that the IBFD is applicable.

$$R_u^{\mathrm{UL,FD}} = R_u^{\mathrm{UL,HD}}, \tag{8}$$

where $R_u^{\mathrm{UL,FD}}$ and $R_u^{\mathrm{UL,HD}}$ are the instantaneous user throughputs estimated using $\gamma_{\Psi,u}^{\mathrm{HD,UL}}$ and $\gamma_{\Psi,u}^{\mathrm{FD,UL}}$, respectively. If (8) is satisfied, the UE to be allocated for superimposed DL communication is determined from the following UE set, $\mathscr{D}_u^{\mathrm{FD}}$, using the PFS algorithm based on the SINR shown in (3):

$$\mathscr{D}_u^{\mathrm{FD}} = \left\{\varphi_i \in \mathscr{D} \middle| R_{\varphi_i,u}^{\mathrm{DL,FD}} \neq 0\right\}. \tag{9}$$

If $\mathscr{D}_u^{\mathrm{FD}} = \varnothing$, IBFD is not applied in this DLSF. These procedures for determining the applicability of IBFD and scheduling in ULSF are shown in Algorithm 2 as pseudo-code.

III. PROPOSED DDC SYSTEM WITH DT AND DISTRIBUTED MULTIPLE RRS

In this section, we present the proposed DDC system with a DT and multiple distributed RRs.

A. OUTLINE OF THE PROPOSED DDC SYSTEM

In the proposed DDC system, the transmitting and reception functions of the RU are separated into DT and RR, respectively, and multiple RRs are distributed in the cell. To enable coordinated operation, the DT and multiple RRs are connected to the CU and DU via a backbone network using RoF technology, similar to RU or RRH. By separating the DT and RR and installing them far apart, it is expected that the effective SI can be significantly reduced. In addition, because the DT and RRs are connected to the same CU and DU through the backbone network, conventional SI cancellation schemes in the digital domain can be used together. Furthermore, by distributing

Algorithm 1: UE Allocation Procedure in DLSF in the DDC System.

1: Estimate $\gamma_{\varphi_i,\Psi}^{\mathrm{HD,DL}}$ for all $\varphi_i \in \mathscr{D}$
2: Choose one φ_i from $\mathscr{D}$ by PFS based on $\gamma_{\varphi_i,\Psi}^{\mathrm{HD,DL}}$ and set $d = \varphi_i$
3: Estimate $\gamma_{d,\Psi,\varphi_j}^{\mathrm{FD,DL}}$ and $\gamma_{\Psi,\varphi_j}^{\mathrm{FD,UL}}$ for all $\varphi_j \in \mathscr{U}$
4: **If** $\mathscr{U}_d^{\mathrm{FD}} := \left\{\varphi_j \in \mathscr{U} | R_d^{\mathrm{DL,\,HD}} = R_{d,\varphi_j}^{\mathrm{DL,FD}} \bigwedge R_{\varphi_j}^{\mathrm{UL,FD}} \neq 0\right\}$ is not an empty set **then**
5: Choose one φ_j from $\mathscr{U}_d^{\mathrm{FD}}$ by PFS based on $\gamma_{\Psi,\varphi_j}^{\mathrm{FD,UL}}$ and set $u = \varphi_j$
6: **End If**
7: **End Procedure**

Algorithm 2: UE Allocation Procedure in ULSF in the DDC System.

1: Estimate $\gamma_{\Psi,\varphi_i}^{\mathrm{HD}}$ for all $\varphi_i \in \mathscr{U}$
2: Choose one φ_i from $\mathscr{U}$ by PFS based on $\gamma_{\Psi,\varphi_i}^{\mathrm{HD,UL}}$ and set $u = \varphi_i$
3: Estimate $\gamma_{\Psi,u}^{\mathrm{FD,UL}}$ and $\gamma_{\varphi_j,\Psi,u}^{\mathrm{FD,DL}}$ for all $\varphi_j \in \mathscr{D}$
4: **If** $R_u^{\mathrm{UL,FD}} = R_u^{\mathrm{UL,HD}}$ **then**
5: Choose one φ_j from $\mathscr{D}_u^{\mathrm{FD}} := \left\{\varphi_j \in \mathscr{D} | R_{\varphi_j,u}^{\mathrm{DL,FD}} \neq 0\right\}$ by PFS based on $\gamma_{\varphi_j,\Psi,u}^{\mathrm{FD,DL}}$ and set $d = \varphi_j$
6: **End If**
7: **End Procedure**

multiple RRs, the propagation distance of UL communication is shortened, and the path loss is reduced, resulting in an improved SINR of the UL communication. These effects are expected to significantly improve the throughput enhancement performance of the DDC system with the introduction of the IBFD.

B. INTERFERENCE MODEL

Fig. 2(b) shows the intracell interference model when the IBFD is applied in the proposed DDC system. The DT antenna of the proposed DDC system is installed at the location of the RU antenna of the conventional DDC system. Therefore, the SINR of the DL communication in HD at DL-UE d, $\gamma_{d,\Psi}^{\mathrm{HD,DL,P}}$, is the same as $\gamma_{d,\Psi}^{\mathrm{HD,DL}}$ in (1). In addition, when a UL-UE u, transmits the UL signal to an RR Ψ_i ($i = 1,\ 2, \ldots, N_{\mathrm{RR}}$), the SINR of UL communication in HD at the RR Ψ_i, is expressed as

$$\gamma_{\Psi_i,u}^{\mathrm{HD,UL,P}} = \frac{G_{u,\Psi_i} L_{\Psi_i,u} G_{\Psi_i,u} P_u}{N_{\Psi_i} B}, \tag{10}$$

where N_{RR} is the number of multiple RRs in the cell.

When DL-UE, d, and UL-UE, u, are simultaneously allocated communications by the application of IBFD, the SINR of DL communication $\gamma_{d,\Psi,u}^{\mathrm{FD,DL,P}}$ is the same as $\gamma_{d,\Psi,u}^{\mathrm{FD,DL}}$ in (3), and the SINR of UL communication received by Ψ_i is expressed as

$$\gamma_{\Psi_i,u}^{\mathrm{FD,UL,P}} = \frac{G_{u,\Psi_i} L_{\Psi_i,u} G_{\Psi_i,u} P_u}{N_{\Psi_i} B + C G_{\Psi,\Psi_i} L_{\Psi_i,\Psi} G_{\Psi_i,\Psi} P_\Psi}. \tag{11}$$

C. UL COMMUNICATION RECEPTION

In the proposed system, the UL communication is received at multiple RRs. The received signals are transmitted to the CU/DU via the backbone network. In this study, it is assumed that the signal received at the RR with the highest SINR is selected, and demodulation processing is performed (which corresponds to receiving the UL communication using the RR with the best reception quality). Therefore, the SINR that determines the quality of UL communication in HD, $\gamma_{\Psi,u}^{\mathrm{HD,UL,P}}$, is expressed as

$$\gamma_{\Psi,u}^{\mathrm{HD,UL,P}} = \max_{i=1,2,\ldots,N_{\mathrm{RR}}} \gamma_{\Psi_i,u}^{\mathrm{HD,UL,P}}. \tag{12}$$

Similarly, the SINR that determines the quality of the UL communication in IBFD, $\gamma_{\Psi,u}^{\mathrm{FD,UL,P}}$, is expressed as

$$\gamma_{\Psi,u}^{\mathrm{FD,UL,P}} = \max_{i=1,2,\ldots,N_{\mathrm{RR}}} \gamma_{\Psi_i,u}^{\mathrm{FD,UL,P}}. \tag{13}$$

D. SCHEDULING AND DETERMINATION OF IBFD APPLICABILITY

Procedures for user scheduling and determination of IBFD applicability in the proposed DDC system are the same as that shown in Section II-C, using the SINR of UL communication selected in (12) and (13). As for the condition for the application of IBFD in ULSF shown in (8), the SINR of the UL communication after the application of IBFD is selected again in (13). Therefore, in the proposed DDC system, the RR that receives the UL signal used for demodulation may differ for the IBFD and HD cases. Pseudo-codes for these procedures are shown in Algorithm 3 for DLSF and in Algorithm 4 for ULSF.

E. POWER CONTROL

1) UL POWER CONTROL

In this study, the Tx power of the UE is determined by an open-loop control based on the Tx power control in the 5G physical uplink shared channel [35]. In the ULSF, the Tx power of u, P_u^{ULSF}, is calculated as follows:

$$P_u^{\mathrm{ULSF}} = \min\left\{P_0 + \alpha \Gamma_{\Psi,u} + 10\log_{10}\left(2^\mu M\right),\ P_u^{\max}\right\}, \tag{14}$$

where P_0 is the target Rx power per physical resource block in the case of a subcarrier spacing of 15 kHz, $\Gamma_{\Psi,u}$ is the amount of attenuation considering antenna gain and path loss, $\alpha \in [0, 1]$ is a coefficient for adjusting the amount of compensation for $\Gamma_{\Psi,u}$, μ is an index of numerology that satisfies $\Delta f = 15 \times 2^\mu$ for the subcarrier spacing Δf kHz, M is the number of allocated resource blocks, and $P_u^{\max}$ is the maximum Tx power of u. In a multicell environment, α is set to reduce intercell interference with the surrounding cells.

Algorithm 3: UE allocation procedure in DLSF in the proposed DDC system.

1: Estimate $\gamma_{\varphi_i,\Psi}^{\mathrm{HD,DL,P}}$ for all $\varphi_i \in \mathscr{D}$
2: Choose one φ_i from $\mathscr{D}$ by PFS based on $\gamma_{\varphi_i,\Psi}^{\mathrm{HD,DL,P}}$ and set $d = \varphi_i$
3: Estimate $\gamma_{d,\Psi,\varphi_j}^{\mathrm{FD,DL,P}}$ and $\gamma_{\Psi,\varphi_j}^{\mathrm{FD,UL,P}}$ for all $\varphi_j \in \mathscr{U}$
4: **If** $\mathscr{U}_d^{\mathrm{FD}} := \left\{\varphi_j \in \mathscr{U} | R_d^{\mathrm{DL,HD}} = R_{d,\varphi_j}^{\mathrm{DL,FD}} \bigwedge R_{\varphi_j}^{\mathrm{UL,FD}} \neq 0\right\}$ is not an empty set **then**
5: Choose one φ_j from $\mathscr{U}_d^{\mathrm{FD}}$ by PFS based on $\gamma_{\Psi,\varphi_j}^{\mathrm{FD,UL,P}}$ and set $u = \varphi_j$
6: **End If**
7: **End Procedure**

Algorithm 4: UE Allocation Procedure in ULSF in the Proposed DDC System.

1: Estimate $\gamma_{\Psi,\varphi_i}^{\mathrm{HD,UL,P}}$ for all $\varphi_i \in \mathscr{U}$
2: Choose one φ_i from $\mathscr{U}$ by PFS based on $\gamma_{\Psi,\varphi_i}^{\mathrm{HD,UL,P}}$ and set $u = \varphi_i$
3: Estimate $\gamma_{\Psi,u}^{\mathrm{FD,UL,P}}$ and $\gamma_{\varphi_j,\Psi,u}^{\mathrm{FD,DL,P}}$ for all $\varphi_j \in \mathscr{D}$
4: **If** $R_u^{\mathrm{UL,FD}} = R_u^{\mathrm{UL,HD}}$ **then**
5: Choose one φ_j from $\mathscr{D}_u^{\mathrm{FD}} := \left\{\varphi_j \in \mathscr{D} | R_{\varphi_j,u}^{\mathrm{DL,FD}} \neq 0\right\}$ by PFS based on $\gamma_{\varphi_j,\Psi,u}^{\mathrm{FD,DL,P}}$ and set $d = \varphi_j$
6: **End If**
7: **End Procedure**

However, because this study assumes a single-cell environment, α is fixed at one. $\Gamma_{\Psi,u}$ in the conventional system is expressed as

$$\Gamma_{\Psi,u} = -10\log_{10}\ G_{u,\Psi}\, L_{\Psi,u}\, G_{\Psi,u}. \tag{15}$$

In the proposed system, the smallest value of attenuation for multiple RRs is used as follows:

$$\Gamma_{\Psi,u} = \min_{i=1,\ldots,N_{\mathrm{RR}}} \left(-10\log_{10}\ G_{u,\Psi_i}\, L_{\Psi_i,u}\, G_{\Psi_i,u}\right). \tag{16}$$

In DLSF, the quality of superimposed UL communication deteriorates by SI from DL communication, unlike the UL communication performed in ULSF. To compensate for this deterioration, the Tx power of the UL-UE in the DLSF, P_u^{DLSF}, is determined by adding an offset term ΔP_0 to (14) to improve the throughput of UL communication as follows:

$$P_u^{\mathrm{DLSF}} = \min\left\{P_0 + \Delta P_0 + \alpha\Gamma_{\Psi,u} + 10\log_{10}\left(2^{\mu}M\right),\ P_u^{\max}\right\}. \tag{17}$$

In a multicell environment, ΔP_0 can increase the interference with surrounding cells. However, this effect is not apparent in the results because a single-cell environment is assumed.

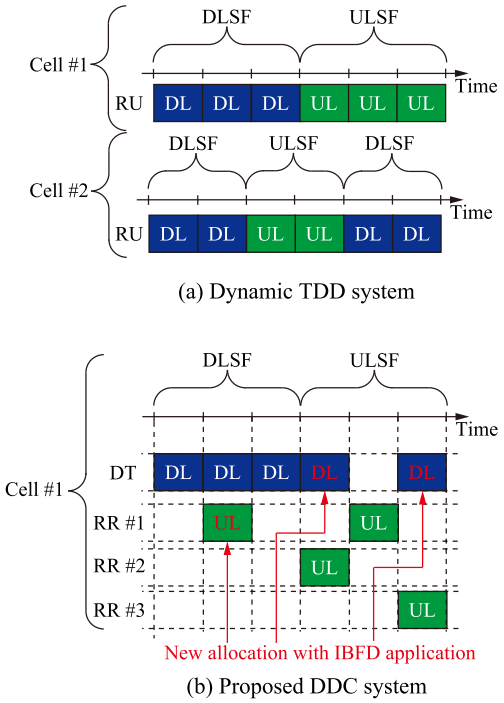

FIGURE 4. Difference between the proposed DDC system and dynamic-TDD system.

2) DL POWER CONTROL

In 5G, the Tx power of the RU is not dynamically controlled. In this study, the Tx power of the RU/DT in the DLSF, P_{Ψ}^{DLSF}, is set to the maximum Tx power of the RU/DT. However, for the DL communication superimposed on the ULSF, the SI provided to the UL communication increases when the Tx power of the RU/DT is large, resulting in a decrease in the IBFD application rate. Therefore, the Tx power of the RU/DT in ULSF, P_{Ψ}^{ULSF}, should be set to a lower value than P_{Ψ}^{DLSF}. However, an excessively low P_{Ψ}^{ULSF} results in low-quality DL communication, which cannot improve the throughput. Therefore, in this study, the optimal Tx power of RU/DT in ULSF, $P_{\Psi}^{\mathrm{ULSF,opt}}$, which maximizes the average user throughput of DL, is obtained for both the conventional and proposed systems and then used for comparative evaluation.

F. DIFFERENCE BETWEEN PROPOSED DDC SYSTEM AND DYNAMIC TDD SYSTEM

As explained in the previous subsections, DT and RRs are separated and placed in a cell in the proposed DDC system. In the subframe where IBFD is applied, DL signal transmission by DT and UL signal reception by RR are performed simultaneously. Although this appears similar to the behavior of the dynamic-TDD system [30], [41], [42], [43], they are different. Here, we clarify the difference between them.

Fig. 4(a) shows the example of subframe allocation in the dynamic-TDD system with a two-cell configuration. Cell #1 and cell #2 have different DLSF and ULSF allocations based on the dynamic-TDD mechanism. Therefore, depending on the subframe, DL and UL are performed simultaneously in

adjacent cells. However, the BSs in cell #1 and cell #2 do not actively cooperate in canceling the interference from DL to UL (i.e., inter-cell interference) and the interference from UL to DL (i.e., IUI) [30], [41], [42], [43].

Fig. 4(b) shows the example of subframe allocation in the proposed DDC system with a single-cell configuration when $N_{\mathrm{RR}} = 3$. The interference from DL to UL (i.e., SI) can be canceled at the DU using classical SI cancellation techniques because the DT and RRs can cooperate, and the interference from UL to DL (i.e., IUI) can be avoided using the proposed UE scheduling scheme.

Furthermore, unlike the proposed DDC system, the dynamic TDD system is only a conventional TDD system in the case of a single cell, which is assumed to be a minimal configuration of local 5G [33], [34] and a hotspot-like deployment.

IV. EVALUATION OF PROPOSED DDC SYSTEM BY COMPUTER SIMULATIONS

The performance of the proposed DDC system was evaluated using computer-based link- and system-level simulations. First, the optimal Tx power in the ULSF at the RU/DT for the conventional and proposed DDC systems was determined. Thereafter, the impact of the target Rx power in the DLSF on the performance was confirmed. Finally, the performance of the proposed DDC system was evaluated, and its effectiveness was shown.

A. SIMULATION CONFIGURATIONS

The evaluation was performed in a single-cell environment, which is assumed to be a minimal configuration of the local 5G [33], [34] or a hotspot-like deployment in a dense urban environment, as shown in Fig. 5. The basic cell configuration was based on the 3rd Generation Partnership Project (3GPP) dense urban scenario macro cell configured in [39], using only one of those sectors. Fig. 5(a) shows the cell configuration of the conventional system. For the proposed system, we evaluated the cases $N_{\mathrm{RR}} = 1$, 3, and 6, as shown in Fig. 5(b)-(d). Table 1 lists the parameters of the simulation based on the 3GPP dense urban scenario [39]. The carrier frequency and system bandwidth were adapted to the technical specifications of the local 5G in Japan [45]. In one loop of the simulation, 10 UEs were uniformly placed in the cell, and operations were performed over 1,000 subframes. After all the loops were executed, the throughput and IBFD application rates were calculated. Because the full buffer model was used for the traffic model, both $\mathscr{U}$ and $\mathscr{D}$ were equal to $\mathscr{N}$. UE communication in each subframe uses the entire system bandwidth.

All UEs are outdoors, and these movements during a loop are not considered. For the received power fluctuation, an additive white Gaussian noise (AWGN) environment, in which only shadowing is considered, was assumed as an initial study. The MCS to be used was selected from the 4 bits channel quality indicator (CQI) table [46] presented in Table 2. In addition, Table 2 lists the SINR regions for which MCS was selected, as calculated by link-level simulations. For this calculation, the required block error rate (BLER) was set to 10^{-1}. The SINRs

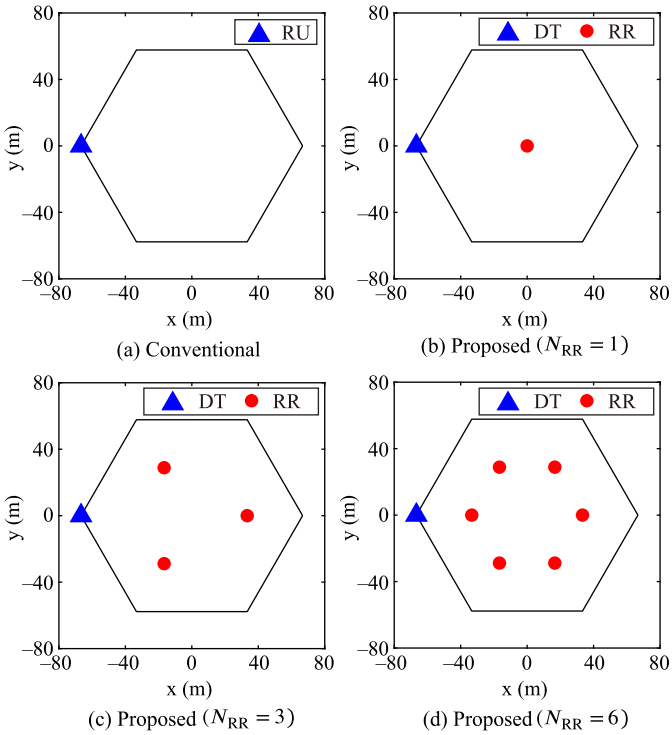

FIGURE 5. Cell configuration.

TABLE 1 Simulation Parameters

Parameters	Values
Carrier frequency	4.8 GHz (e.g., Local 5G, Japan)
Subcarrier spacing	15 kHz
System bandwidth	40 MHz (e.g., Local 5G, Japan)
Available resource blocks	216
Thermal noise power	–98 dBm
Base duplex scheme	TDD (DL:UL = 5:5)
Path loss (DT–RR)	3GPP, 3D-UMa [40]
Path loss (RU/DT–UE)	3GPP, 3D-UMa [40]
Path loss (RR–UE)	3GPP, 3D-UMa [40]
Path loss (UE–UE)	3GPP, A2.1.2 Outdoor to Outdoor in [44]
Penetration loss	0
Shadowing correlation	0
Channel	AWGN
Scheduling scheme	PFS
Traffic model	Full buffer model
Number of loops	1,000

shown in (1)–(4), (10), and (11) were assumed to be ideally estimated.

Table 3 lists the specifications of the UE, RU/DT, and RR of the evaluated systems. For simplicity, a single-input single-output was assumed to be implemented. The amount of SI cancellation in a conventional system was assumed to be 110 dB, as reported in [15], which is obtained by analog and digital domain cancellation. The amount of SI cancellation in the proposed system was assumed to be 50 dB, which is achieved only by cancellation in the digital domain in [15].

TABLE 2 CQI Table

CQI	Modulation	Code rate	Spectral efficiency (bps/Hz)	Available SINR range (Calculated by link-level simulation with the threshold as BLER $\leq 10^{-1}$)
0	Out of range		0	Less than –10.3 dB
1	QPSK	78/1024	0.1523	From –10.3 dB to –8.4 dB
2	QPSK	120/1024	0.2344	From –8.4 dB to –6.4 dB
3	QPSK	193/1024	0.3770	From –6.4 dB to –4.0 dB
4	QPSK	308/1024	0.6016	From –4.0 dB to –1.9 dB
5	QPSK	449/1024	0.8770	From –1.9 dB to 0.1 dB
6	QPSK	602/1024	1.1758	From 0.1 dB to 2.0 dB
7	16QAM	378/1024	1.4766	From 2.0 dB to 3.9 dB
8	16QAM	490/1024	1.9141	From 3.9 dB to 5.8 dB
9	16QAM	616/1024	2.4063	From 5.8 dB to 7.6 dB
10	64QAM	466/1024	2.7305	From 7.6 dB to 9.6 dB
11	64QAM	567/1024	3.3223	From 9.6 dB to 11.3 dB
12	64QAM	666/1024	3.9023	From 11.3 dB to 13.3 dB
13	64QAM	772/1024	4.5234	From 13.3 dB to 15.4 dB
14	64QAM	873/1024	5.1152	From 15.4 dB to 17.8 dB
15	64QAM	948/1024	5.5547	More than 17.8 dB

TABLE 3 Specifications of UE, RU/DT, and RR

Parameters	Values
UE maximum Tx power	23 dBm
UE antenna height	1.5 m
UE antenna pattern / gain	Isotropic / 0 dBi
UE noise figure	9 dB
RU/DT maximum Tx power	44 dBm
RU/DT antenna height	25 m
RU/DT antenna pattern / gain	Directional / 8 dBi
RU/DT noise figure	5 dB
SI cancellation (conventional system)	110 dB
RR antenna height	22.5 m
RR antenna pattern / gain	Omnidirectional / 5 dBi
RR noise figure	5 dB
SI cancellation (proposed system)	50 dB

This is because the implementation of a circulator cannot be assumed in the proposed system as the Tx and Rx antennas are separated, and the implementation of a dedicated circuit for SI cancellation is not considered in this study.

B. OPTIMIZATION OF RU/DT TX POWER IN ULSF

Prior to the evaluation of the user throughput and IBFD application rate, we determined $P_{\Psi}^{\mathrm{ULSF,opt}}$ in the conventional and proposed systems under the condition $\Delta P_0 = 0$ dB.

1) CONVENTIONAL DDC SYSTEM

Fig. 6(a) and (b) show the IBFD application rate and average user throughput, respectively, as functions of P_{Ψ}^{ULSF} in the conventional system. The user throughput of the case where the application of IBFD is not allowed is shown as *HD* for reference. Because the DLSF parameters are independent of P_{Ψ}^{ULSF}, the IBFD application rate for UL communication in

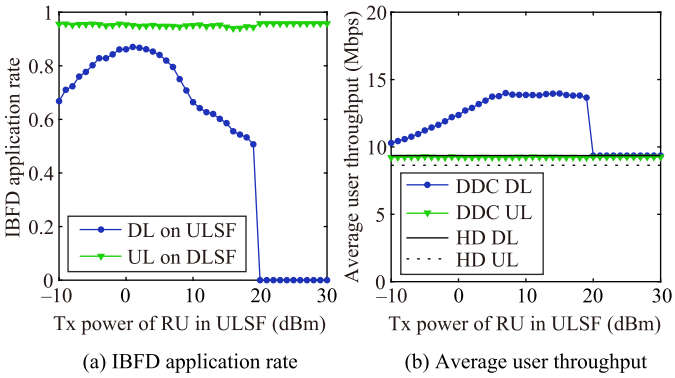

FIGURE 6. Optimization of P_{Ψ}^{ULSF} in the conventional system.

DLSF remains constant, even if P_{Ψ}^{ULSF} is changed. In addition, the quality of the UL communication in the ULSF is guaranteed by (8). Therefore, the average user throughput of UL communication is constant regardless of the P_{Ψ}^{ULSF}.

For DL communication, in the range of $P_{\Psi}^{\mathrm{ULSF}} \leq 1$ dBm, the IBFD application rate in ULSF and the average user throughput improved with an increase in P_{Ψ}^{ULSF}. This is because, as P_{Ψ}^{ULSF} increases, the SINR of DL communication in ULSF improves, and consequently, the number of UEs that satisfy the condition of $R_{\varphi_i,u}^{\mathrm{DL,IBFD}} \neq 0$ in (9) increases. However, depending on the location of the UL-UE, the residual SI component can still degrade the UL communication quality, even with the assumption of 110 dB SI cancellation. Therefore, the IBFD application rate does not reach one because the condition for IBFD application in ULSF shown in (8) is not always satisfied.

In the range of 2 dBm $\leq P_{\Psi}^{\mathrm{ULSF}} \leq$ 19 dBm, the IBFD application rate in ULSF decreased as P_{Ψ}^{ULSF} increased. This is because the residual SI component increases and degrades the SINR of UL communication with the increase in P_{Ψ}^{ULSF}, increasing the number of ULSFs where (8) is not satisfied. However, as P_{Ψ}^{ULSF} increases, the quality of the superimposed DL communication in ULSF improves. Consequently, the average user throughput of the DL communication reaches a maximum value at $P_{\Psi}^{\mathrm{ULSF}} = 7$ dBm and remains almost constant at 7 dBm $\leq P_{\Psi}^{\mathrm{ULSF}} \leq 19$ dBm.

In the range of $P_{\Psi}^{\mathrm{ULSF}} \geq 20$ dBm, even if the Tx power of the UL-UE does not reach $P_u^{\max}$ in ULSF, the target receiving power in (14) is achieved, the degradation of UL communication quality owing to the residual SI component occurs, and (8) is not satisfied. Therefore, IBFD cannot be applied to ULSF, and the average user throughput of DL communication is equivalent to that of a TDD system using HD. Consequently, $P_{\Psi}^{\mathrm{ULSF,opt}}$ in the conventional system was determined to be 7 dBm.

2) PROPOSED DDC SYSTEM

Figs. 7, 8, and 9 show the IBFD application rate and average user throughput in the proposed system as functions of P_{Ψ}^{ULSF}. When $N_{\mathrm{RR}} = 1$, as shown in Fig. 7, the IBFD application rate

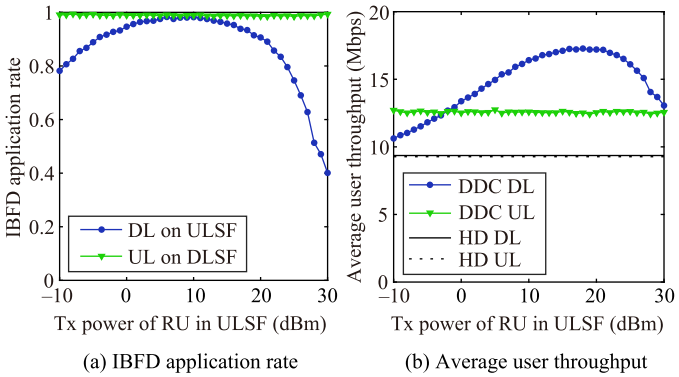

(a) IBFD application rate (b) Average user throughput

FIGURE 7. Optimization of P_{Ψ}^{ULSF} in the proposed system ($N_{\mathrm{RR}} = 1$).

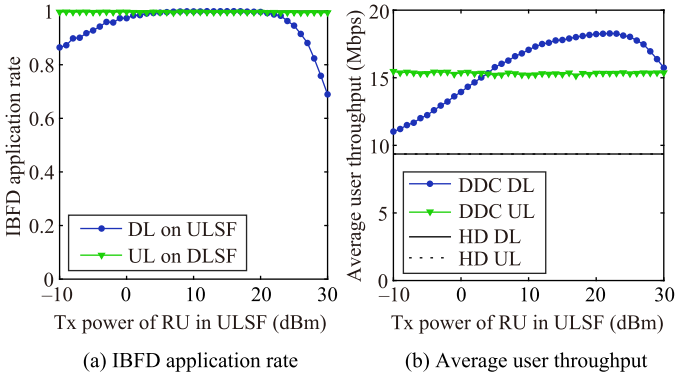

(a) IBFD application rate (b) Average user throughput

FIGURE 8. Optimization of P_{Ψ}^{ULSF} in the proposed system ($N_{\mathrm{RR}} = 3$).

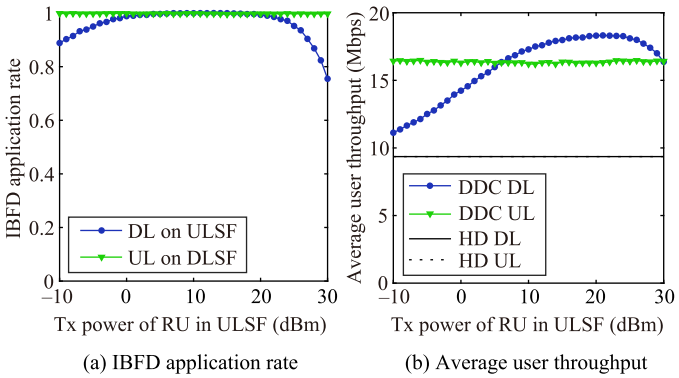

(a) IBFD application rate (b) Average user throughput

FIGURE 9. Optimization of P_{Ψ}^{ULSF} in the proposed system ($N_{\mathrm{RR}} = 6$).

increases in the range of $P_{\Psi}^{\mathrm{ULSF}} \leq 10$ dBm. This is because the number of UEs satisfying the conditions $R_{\varphi_i,u}^{\mathrm{DL,FD}} \neq 0$ in (9) increases as P_{Ψ}^{ULSF} increases. In the conventional system, the IBFD application rate cannot reach one owing to insufficient SI cancellation. However, in the proposed system, the IBFD application rate can reach approximately one because the SI is small owing to the path loss between the DT and RR, and the residual SI is also sufficiently small.

In the range of $P_{\Psi}^{\mathrm{ULSF}} \geq 11$ dBm, the IBFD application rate decreases because the number of ULSFs where (8) is not satisfied increases owing to the increase in residual SI. However, as the quality of DL communication superimposed on ULSF improves, the average user throughput of DL communication increases. The average user throughput of DL communication is maximum at $P_{\Psi}^{\mathrm{ULSF}} = 18$ dBm and decreases when P_{Ψ}^{ULSF} is further increased. Therefore, the optimal value of P_{Ψ}^{ULSF} in the proposed system, where $N_{\mathrm{RR}} = 1$ is determined as $P_{\Psi}^{\mathrm{ULSF,opt}} = 18$ dBm.

In the cases $N_{\mathrm{RR}} = 3$ and 6, as shown in Figs. 8 and 9, the IBFD application rate improves for any P_{Ψ}^{ULSF} compared to the case $N_{\mathrm{RR}} = 1$ because the RR with a smaller SI can be selected from multiple RRs, as in (13), and it is easier to satisfy (8). The average user throughput of the DL communication reaches its maximum value at $P_{\Psi}^{\mathrm{ULSF}} = 22$ dBm for $N_{\mathrm{RR}} = 3$ and $P_{\Psi}^{\mathrm{ULSF}} = 21$ dBm for $N_{\mathrm{RR}} = 6$. Therefore, the optimal values of P_{Ψ}^{ULSF} for $N_{\mathrm{RR}} = 3$ and $N_{\mathrm{RR}} = 6$ were determined as $P_{\Psi}^{\mathrm{ULSF,opt}} = 22$ dBm and $P_{\Psi}^{\mathrm{ULSF,opt}} = 21$ dBm, respectively.

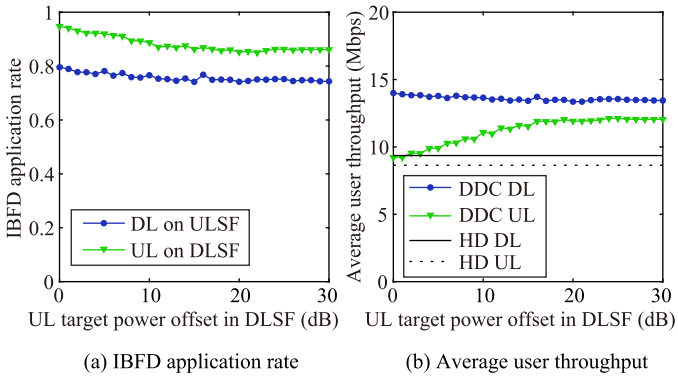

(a) IBFD application rate (b) Average user throughput

FIGURE 10. Impacts of ΔP_0 in the conventional system.

C. IMPACTS OF RU/RR TARGET RX POWER IN DLSF

The impacts of ΔP_0 on the performances were confirmed under the conditions $P_{\Psi}^{\mathrm{ULSF}} = P_{\Psi}^{\mathrm{ULSF,opt}}$.

1) CONVENTIONAL SYSTEM

Fig. 10(a) and (b) show the IBFD application rate and average user throughput, respectively, as functions of ΔP_0 in the conventional system. In the range of $\Delta P_0 \leq 15$ dB, the IBFD application rate in the DLSF decreased as ΔP_0 increased. This is because IUI provided to the DL-UE increases as the Tx power of the UL-UE increases, and the number of UEs satisfying the condition $R_d^{\mathrm{DL,\,HD}} = R_{d,\varphi_i}^{\mathrm{DL,FD}}$ in (7) decreases. However, the increase in ΔP_0 improves the average user throughput of UL communication because it enables the superimposition of high-quality UL communication when IBFD is applied.

In ULSF, the IBFD application rate decreased slightly with increasing ΔP_0. Because UEs far from the RU reach the upper limit of the Tx power even when ΔP_0 is approximately 0 dB, increasing ΔP_0 does not change the communication quality. Therefore, in the DLSF, UEs closer to the RU have a relatively larger metric on the right-hand side of (5) and are more likely to be allocated. Conversely, in ULSF, the allocation to the UEs far from the RU is increased to meet

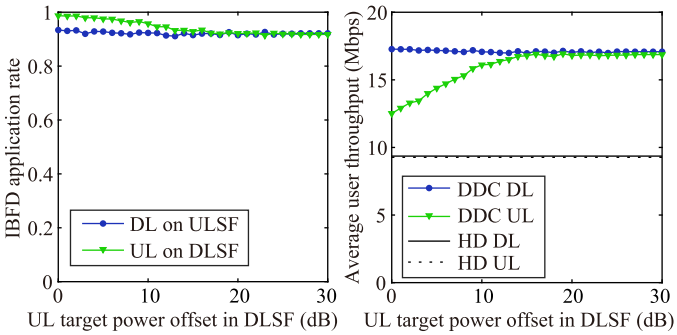

(a) IBFD application rate (b) Average user throughput

FIGURE 11. Impacts of ΔP_0 in the proposed system ($N_{\mathrm{RR}} = 1$).

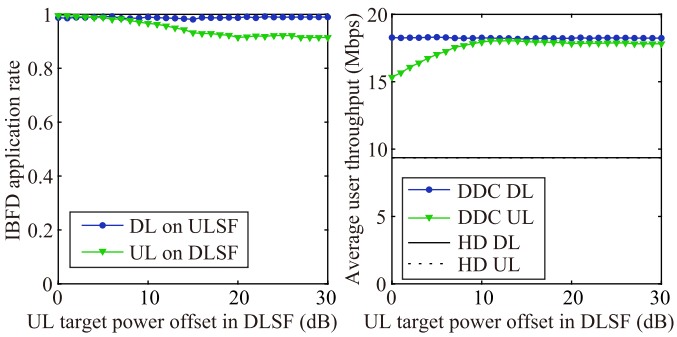

(a) IBFD application rate (b) Average user throughput

FIGURE 12. Impacts of ΔP_0 in the proposed system ($N_{\mathrm{RR}} = 3$).

the PFS rule. When the UEs cannot achieve the UL target Rx power allocated, it becomes difficult to satisfy (8), which is the condition for superimposing DL communication. Therefore, the IBFD application rate in ULSF decreased. In the range of $\Delta P_0 \geq 16$ dB, the IBFD application rate and average user throughput of UL communication in DLSF are almost constant. This is because the number of UEs for which $P_u^{\max}$ is selected in (17) increases as ΔP_0 increases, whereas P_u^{ULSF} and P_u^{DLSF} remain unchanged.

2) PROPOSED SYSTEM

Fig. 11 shows the IBFD application rate and average user throughput as a function of ΔP_0 when $N_{\mathrm{RR}} = 1$ in the proposed system. In the range of $\Delta P_0 \leq 10$ dB, the IBFD application rate in the DLSF decreases, as in the conventional system, because of the increase in IUI with the increase in ΔP_0. However, because $\Gamma_{\Psi,u}$ in (17) is on average smaller than that in the conventional system, there are relatively few cases where the UE Tx power reaches its upper limit, and the UL communication quality does not improve. Consequently, the average user throughput of UL communication is significantly increased. In the range of $\Delta P_0 \geq 21$ dB, both the IBFD application rate in the DLSF and the average user throughput of UL communication remain constant as more UEs reach the upper limit of the Tx power.

Fig. 12 shows the IBFD application rate and average user throughput as a function of ΔP_0 when $N_{\mathrm{RR}} = 3$ in the proposed system. In the range of $\Delta P_0 \leq 8$ dB, the IBFD application rate in the DLSF does not decrease when ΔP_0 is increased, unlike in the conventional system. Because the $\Gamma_{\Psi,u}$ is smaller than that in the conventional system, and the UL-UE transmit power is lower, thus there are many UL-UE candidates—UEs that satisfy the condition $R_d^{\mathrm{DL,\,HD}} = R_{d,\varphi_i}^{\mathrm{DL,FD}}$ in (7), even when ΔP_0 is large. An increase in ΔP_0 improves the quality of the UL communication superimposed on the DLSF, resulting in a higher average user throughput of UL communication. In the range of 9 dB $\leq \Delta P_0 \leq$ 20 dB, the average user throughput of UL communication does not improve because the IBFD application rate in DLSF decreases owing to an increase in IUI. In the range of $\Delta P_0 \geq 21$ dB, both the IBFD application rate in the DLSF and the average user throughput of UL communication remain constant because the number of cases where the maximum Tx power of the UE is reached increases.

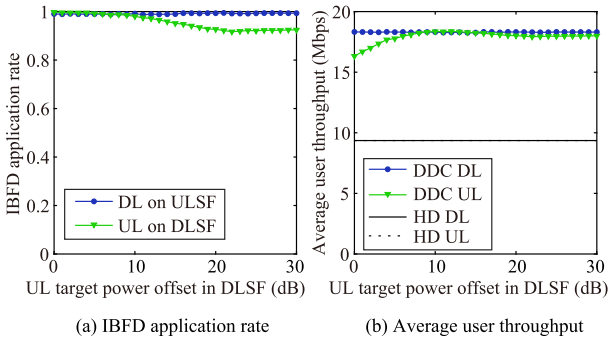

(a) IBFD application rate (b) Average user throughput

FIGURE 13. Impacts of ΔP_0 in the proposed system ($N_{\mathrm{RR}} = 6$).

Fig. 13 shows the IBFD application rate and average user throughput as a function of ΔP_0 when $N_{\mathrm{RR}} = 6$ in the proposed system. The variation in the IBFD application rate in DLSF and the average user throughput for UL communication with respect to ΔP_0 show the same trend as in the case of $n_{\mathrm{RR}} = 3$. The average user throughput of UL communication improved in the range of $\Delta P_0 \leq 10$ dB. For example, a 0.98 Mbps improvement at $\Delta P_0 = 0$ dB and a 0.41 Mbps improvement at $\Delta P_0 = 10$ dB. This is because, as the number of RR increases, the distance between the UL-UE and RR decreases on average, resulting in cases where the UL received signal with a higher SINR can be selected in (13).

D. COMPREHENSIVE PERFORMANCE EVALUATION

As mentioned above, it was confirmed that increasing ΔP_0 improves the average user throughput of UL communication for both conventional and proposed systems. However, it is desirable to reduce ΔP_0 from the viewpoint of UE power consumption. In this section, we perform a comprehensive evaluation and comparison of the IBFD application rate and user throughput (average and 5% outage) of the conventional and proposed DDC systems when ΔP_0 is set to 0 dB and 10 dB, as shown in Table 4. To separately confirm the effects of shortening the UL propagation distance and reducing self-interference, the results for the case where the application of

TABLE 4 IBFD Application Rate and User Throughput

System	IBFD application	UL target receiving power offset in DLSF, ΔP_0	IBFD application rate		Average user throughput (Mbps)		5% user throughput (Mbps)	
			UL on DLSF	DL on ULSF	UL	DL	UL	DL
Conventional	Not allowed (i.e., Existing HD)	N/A	N/A	N/A	8.64	9.36	4.60	9.36
	Allowed (i.e., Conventional DDC)	0 dB	0.95	0.80	9.23	14.00	4.88	11.04
		10 dB	0.89	0.77	11.08	13.66	5.98	10.67
Proposed ($N_{RR} = 1$)	Not allowed	N/A	N/A	N/A	9.27	9.36	9.17	9.36
	Allowed	0 dB	0.99	0.93	12.51	17.27	10.15	14.04
		10 dB	0.92	0.96	15.97	17.12	12.07	13.62
Proposed ($N_{RR} = 3$)	Not allowed	N/A	N/A	N/A	9.36	9.36	9.36	9.36
	Allowed	0 dB	1.00	0.99	15.34	18.28	11.77	15.72
		10 dB	0.97	0.99	17.94	18.26	13.17	15.72
Proposed ($N_{RR} = 6$)	Not allowed	N/A	N/A	N/A	9.36	9.36	9.36	9.36
	Allowed	0 dB	1.00	0.99	16.32	18.32	11.67	15.91
		10 dB	0.99	0.98	18.35	18.31	13.48	15.71

IBFD is not allowed for both the conventional and proposed DDC systems are also shown. The case where the application of IBFD is not allowed in the conventional DDC system is equivalent to the case of the existing HD system.

1) CASE WHERE THE APPLICATION OF IBFD IS NOT ALLOWED

In the case where the application of IBFD is not allowed, the proposed system improves the average user throughput and 5th percentile outage user throughput (5% user throughput) of UL communication by 7% and 99%, respectively, for $N_{RR} = 1$, and by 8% and 103%, respectively, for $N_{RR} = 3$ and 6. This performance is achieved because the distance between the UL-UE and RR in the RR-distributed topology is smaller than the distance between the UL-UE and RU in the conventional topology, which allows the UL-UE to achieve the target Rx power without reaching the maximum Tx power, particularly at the cell edge. Thus, improving the SINR of UL communication allows the MCS with higher spectral efficiency to be used.

2) CASE WHERE THE APPLICATION OF IBFD IS ALLOWED

In the case where the application of IBFD is allowed, the IBFD application rate in ULSF is only 0.8 owing to insufficient SI cancellation, even when P_{Ψ}^{ULSF} is optimized in the conventional system. Furthermore, because $P_{\Psi}^{\mathrm{ULSF,opt}}$ is as small as 7 dBm, the average user throughput improvement for DL communication compared with the case where the application of IBFD is not allowed is 50%.

The proposed DDC system where P_{Ψ}^{ULSF} is optimized can raise the IBFD application rate in ULSF to 0.93 for $N_{RR} = 1$ and 0.99 for $N_{RR} = 3$ and 6, in contrast to the conventional DDC system, because SI can be significantly reduced by separating the Tx and Rx functions of the RU. In addition, the average user throughput is improved by 85% for $N_{RR} = 1$, 95% for $N_{RR} = 3$, and 96% for $N_{RR} = 6$, compared with the case where the application of IBFD is not allowed because $P_{\Psi}^{\mathrm{ULSF,opt}}$ is sufficiently large to ensure the quality of the superimposed DL communication. These results are close to 100%, which is the ideal value for the improvement rate by the application of IBFD.

The average user throughput of UL communication is also improved by 35% for $N_{RR} = 1$, 64% for $N_{RR} = 3$, and 74% for $N_{RR} = 6$, whereas only 7% is obtained for the conventional DDC system. This is because the separation of the Tx and Rx functions of the RU significantly reduces the SI and suppresses the degradation of the SINR of the UL communication when IBFD is applied. Furthermore, when ΔP_0 is set to 10 dB, the average user throughput of UL communication in the proposed DDC system is improved by 72% for $N_{RR} = 1$, 92% for $N_{RR} = 3$, and 96% for $N_{RR} = 6$, from the case where the application of IBFD is not allowed. Because the quality of DL communication in the DLSF is guaranteed by (7), the average user throughput of DL communication is equivalent to that of $\Delta P_0 = 0$ dB. This implies that the proposed DDC system can achieve a user throughput close to twice that of the case where the application of IBFD is not allowed for both DL and UL communications, which is the ideal value of IBFD. In addition, compared to the case where the application of IBFD is not allowed in the conventional DDC system, which is equivalent to the case of the existing HD system, the average user throughput enhancement of the proposed DDC system where $\Delta P_0 = 10$ dB and $N_{RR} = 3$ are 108% for UL communication and 95% for DL communication; the average user throughput enhancement where $\Delta P_0 = 10$ dB and $N_{RR} = 6$ are 112% for UL communication and 96% for DL communication. These results indicate that increasing RRs beyond $N_{RR} = 3$ does not result in linear performance improvement, and setting the number of RRs to $N_{RR} = 3$ is efficient in the assumed circumstance.

V. CONCLUSION AND FUTURE WORKS

In this study, we proposed a DDC system in which the reception function of the RU is distributed in the cell as multiple

simple structured RRs. The proposed DDC system improves the communication quality by reducing the SI generated at the RU when IBFD is applied through path loss and by reducing the propagation distance of the UL communication on average. The effectiveness of the proposed system was evaluated using link- and system-level simulations. Under the conditions of optimizing the Tx power of the DL communication superimposed on ULSF and increasing the UL target Rx power in the DLSF by 10 dB, the proposed DDC system with the RR-distributed topology where six RRs are installed can increase average user throughput by 96% each for the UL and DL communications over HD system with the same topology. Sufficient performance was also confirmed for a smaller number of RRs. The proposed DDC system is expected to further improve the performance by using multiple antenna techniques. Considering inter-cell interference in a multicell environment as a more practical and flexible system and discussing optimality under such complex conditions is a topic for future work. Furthermore, to apply our system to mm-wave communication, IBFD-massive MIMO [47], [48] must be considered in future work.

REFERENCES

[1] K. Fukushima, S. Mori, K. Mizutani, and H. Harada, "Single-cell dynamic duplex cellular system using distributed receive-only base stations," in *Proc. IEEE 95th Veh. Technol. Conf.*, 2022, pp. 1–5.

[2] ARIB 2020 and beyond Ad Hoc Group, "Mobile communications systems for 2020 and beyond," White Paper, Version 1.0.0, Oct. 2014.

[3] Cisco, "Cisco annual internet report (2018–2023)," White Paper, Mar. 2020.

[4] J. G. Andrews et al., "What will 5G be?," *IEEE J. Sel. Areas Commun.*, vol. 32, no. 6, pp. 1065–1082, Jun. 2014.

[5] B. Yang, Z. Yu, J. Lan, R. Zhang, J. Zhou, and W. Hong, "Digital beamforming-based massive MIMO transceiver for 5G millimeter-wave communications," *IEEE Trans. Microw. Theory Techn.*, vol. 66, no. 7, pp. 3403–3418, Jul. 2018.

[6] 3GPP, "Physical channels and modulation," 3GPP Tech. Specification 38.211 V16.7.0, Sep. 2021.

[7] A. Gupta and R. K. Jha, "A survey of 5G network: Architecture and emerging technologies," *IEEE Access*, vol. 3, pp. 1206–1232, 2015.

[8] Z. Zhang, X. Chai, K. Long, A. V. Vasilakos, and L. Hanzo, "Full duplex techniques for 5G networks: Self-interference cancellation, protocol design, and relay selection," *IEEE Commun. Mag.*, vol. 53, no. 5, pp. 128–137, May 2015.

[9] A. A. Amin and S. Y. Shin, "Capacity analysis of cooperative NOMA-OAM-MIMO based full-duplex relaying for 6G," *IEEE Wireless Commun. Lett.*, vol. 10, no. 7, pp. 1395–1399, Jul. 2021.

[10] B. Li, L.-L. Yang, R. G. Maunder, P. Xiao, and S. Sun, "Multicarrier-division duplex: A duplexing technique for the shift to 6G wireless communications," *IEEE Veh. Technol. Mag.*, vol. 16, no. 4, pp. 57–67, Dec. 2021.

[11] F. E. Airod, H. Chafnaji, and H. Yanikomeroglu, "HARQ in full-duplex relay-assisted transmissions for URLLC," *IEEE Open J. Commun. Soc.*, vol. 2, pp. 409–422, 2021.

[12] E. Basar, M. Di Renzo, J. De Rosny, M. Debbah, M.-S. Alouini, and R. Zhang, "Wireless communications through reconfigurable intelligent surfaces," *IEEE Access*, vol. 7, pp. 116753–116773, 2019.

[13] E. Calvanese Strinati et al., "6G: The next frontier: From holographic massaging to artificial intelligence using subterahertz and visible light communication," *IEEE Veh. Technol. Mag.*, vol. 14, no. 3, pp. 42–50, Sep. 2019.

[14] K. Mizutani and H. Harada, "Quantization noise reduction by digital signal processing-assisted analog-to-digital converter for in-band full-duplex systems," *IEEE Trans. Wireless Commun.*, vol. 21, no. 8, pp. 6643–6655, Aug. 2022.

[15] D. Bharadia, E. McMilin, and S. Katti, "Full duplex radios," in *Proc. ACM SIGCOMM Comput. Commun. Rev.*, 2013, pp. 375–386.

[16] S. Hong et al., "Applications of self-interference cancellation in 5G and beyond," *IEEE Commun. Mag.*, vol. 52, no. 2, pp. 114–121, Feb. 2014.

[17] A. Sabharwal, P. Schniter, D. Guo, D. W. Bliss, S. Rangarajan, and R. Wichman, "In-band full-duplex wireless: Challenges and opportunities," *IEEE J. Sel. Areas Commun.*, vol. 32, no. 9, pp. 1637–1652, Sep. 2014.

[18] D. Kim, H. Lee, and D. Hong, "A survey of in-band full-duplex transmission: From the perspective of PHY and MAC layers," *IEEE Commun. Surv. Tut.*, vol. 17, no. 4, pp. 2017–2046, Oct.–Dec. 2015.

[19] M. Jain et al., "Practical, real-time, full-duplex wireless," in *Proc. 17th Annu. Int. Conf. Mobile Comput. Netw.*, 2011, pp. 301–312.

[20] N. Zarifeh, M. Alissa, M. Khaliel, and T. Kaiser, "Self-interference mitigation in full-duplex base-station using dual polarized reflect-array," in *Proc. 11th German Microw. Conf.*, 2018, pp. 180–183.

[21] G. Chaudhary, J. Jeong, and Y. Jeong, "Differential fed antenna with high self-interference cancellation for in-band full-duplex communication system," *IEEE Access*, vol. 7, pp. 45340–45348, 2019.

[22] E. Ahmed and A. M. Eltawil, "All-digital self-interference cancellation technique for full-duplex systems," *IEEE Trans. Wireless Commun.*, vol. 14, no. 7, pp. 3519–3532, Jul. 2015.

[23] K. E. Kolodziej, J. G. McMichael, and B. T. Perry, "Multitap RF canceller for in-band full-duplex wireless communications," *IEEE Trans. Wireless Commun.*, vol. 15, no. 6, pp. 4321–4334, Jun. 2016.

[24] T. Matsumura, H. Kuriki, K. Mizutani, and H. Harada, "Macro-cell capacity enhancement with dynamic full-duplex cellular system," in *Proc. 21st Int. Symp. Wireless Pers. Multimedia Commun.*, 2018, pp. 336–341.

[25] K. Nishikori, K. Teramae, K. Mizutani, T. Matsumura, and H. Harada, "User throughput enhancement with dynamic full-duplex cellular system in dense urban multi-cell environment," in *Proc. IEEE 30th Annu. Int. Symp. Pers., Indoor Mobile Radio Commun.*, 2019, pp. 1–6.

[26] Y. Arakawa, K. Nishikori, K. Mizutani, T. Matsumura, and H. Harada, "An initial study of dynamic-duplex cellular system on 5G NR downlink in high SHF band," in *Proc. IEEE 18th Annu. Consum. Commun. Netw. Conf.*, 2021, pp. 1–2.

[27] S. Mori, K. Mizutani, and H. Harada, "In-band full-duplex-applicable area expansion by inter-user interference reduction using successive interference cancellation," *IEICE Trans. Commun.*, vol. E105-B, no. 2, pp. 168–176, Feb. 2022.

[28] R. Chowdhury and A. K. M. Sharoar Jahan Choyon, "Performance analysis of Tx-Rx isolated distributed antenna system implementing in-band full-duplex for up-link communication to mitigate self-interference in 5G," in *Proc. 1st Int. Conf. Adv. Sci., Eng. Robot. Technol.*, 2019, pp. 1–5.

[29] N. Zarifeh, M. Alissa, T. Kreul, and T. Kaiser, "Antenna selection performance of distributed antenna systems in full-duplex indoor base station," in *Proc. 12th German Microw. Conf.*, 2019, pp. 32–35.

[30] H. Kamboj et al., "Hardware implementation of cell-free MIMO and dynamic TDD using the OAI 5G NR codebase," in *Proc. 25th Int. ITG Workshop Smart Antennas*, 2021, pp. 1–5.

[31] H. A. Ammar, R. Adve, S. Shahbazpanahi, G. Boudreau, and K. V. Srinivas, "User-centric cell-free massive MIMO networks: A survey of opportunities, challenges and solutions," *IEEE Commun. Surv. Tut.*, vol. 24, no. 1, pp. 611–652, Jan.–Mar. 2021.

[32] J. Qiu et al., "Secure transmission scheme based on fingerprint positioning in cell-free massive MIMO systems," *IEEE Trans. Signal Inf. Process. Over Netw.*, vol. 8, pp. 92–105, 2022.

[33] Y. Siriwardhana, P. Porambage, M. Ylianttila, and M. Liyanage, "Performance analysis of local 5G operator architectures for industrial internet," *IEEE Internet Things J.*, vol. 7, no. 12, pp. 11559–11575, Dec. 2020.

[34] Y. Oishi, S. Hayase, and M. Takase, "A study on interconnection between local 5G networks and existing networks," *IEICE Commun. Exp.*, vol. 10, no. 12, pp. 888–893, Dec. 2021.

[35] 3GPP, "Physical layer procedures for control," 3GPP Tech. Specification 38.213 V16.7.0, Sep. 2021.

[36] A. Jalali, R. Padovani, and R. Pankaj, "Data throughput of CDMA-HDR a high efficiency-high data rate personal communication wireless system," in *Proc. IEEE 51st Veh. Technol. Conf.*, 2000, vol. 3, pp. 1854–1858.

[37] R. Kwan, C. Leung, and J. Zhang, "Proportional fair multiuser scheduling in LTE," *IEEE Signal Process. Lett.*, vol. 16, no. 6, pp. 461–464, Jun. 2009.
[38] A. Mamane, M. El Ghazi, S. Mazer, M. Bekkali, M. Fattah, and M. Mahfoudi, "The impact of scheduling algorithms for real-time traffic in the 5G femto-cells network," in *Proc. 9th Int. Symp. Signal, Image, Video Commun.*, 2018, pp. 147–151.
[39] 3GPP, "Study on new radio access technology physical layer aspects," 3GPP Tech. Rep. 38.802 V14.2.0, Sep. 2017.
[40] 3GPP, "Study on 3D channel model for LTE," 3GPP Tech. Rep. 36.873 V12.7.0, Dec. 2017.
[41] L. Xue, Y. Cheng, Y. Zhou, and B. Qu, "Next generation TDD cellular communication," in *Proc. Asilomar Conf. Signals Syst. Comput.*, Nov. 2015, pp. 1036–1040.
[42] J. Liu, R. Fan, H. Wang, J. Liu, and F. Wang, "Dynamic TDD testbed and field measurements," in *Proc. IEEE 83rd Veh. Technol. Conf.*, 2016, pp. 1–5.
[43] Z. Shen, A. Khoryaev, E. Eriksson, and X. Pan, "Dynamic uplink-downlink configuration and interference management in TD-LTE," *IEEE Commun. Mag.*, vol. 50, no. 11, pp. 51–59, Nov. 2012.
[44] 3GPP, "Study on LTE device to device proximity services; radio aspects," 3GPP Tech. Rep. 36.843 V12.0.1, Mar. 2014.
[45] Ministry of Internal Affairs and Communications (MIC), "Announcement of the local 5G implementation guidelines institutional development for local 5G implementation," *Newslett. MIC*, vol. 30, no. 4, pp. 1–3, Dec. 2019.
[46] 3GPP, "User equipment (UE) radio transmission and reception; Part 2: Range 2 standalone," 3GPP Tech. Specification 38.101-2 V17.3.0, Sep. 2021.
[47] X. Xia, K. Xu, Y. Wang, and Y. Xu, "A 5G-enabling technology: Benefits, feasibility, and limitations of in-band full-duplex mMIMO," *IEEE Veh. Technol. Mag.*, vol. 13, no. 3, pp. 81–90, Sep. 2018.
[48] K. Xu, Z. Shen, Y. Wang, X. Xia, and D. Zhang, "Hybrid time-switching and power splitting SWIPT for full-duplex massive MIMO systems: A beam-domain approach," *IEEE Trans. Veh. Technol.*, vol. 67, no. 8, pp. 7257–7274, Aug. 2018.

KEITA FUKUSHIMA (Student Member, IEEE) received the B.E. degree in electric and electrical engineering in 2022 from Kyoto University, Kyoto, Japan, where he is currently working toward the M.I. degree from the Graduate School of Informatics. His research focuses on the topic of in-band full-duplex cellular systems.

SHOTA MORI (Student Member, IEEE) received the B.E. degree in 2021 from the Faculty of Engineering, Kyoto University, Kyoto, Japan, where he is currently working toward the M.I. degree from the Graduate School of Informatics. His research focuses on the topics of physical layer technologies of the 6th generation mobile communication (6G) system. He was the recipient of the Student Paper Award from IEEE VTS Tokyo/Japan Chapter in 2021.

KEIICHI MIZUTANI (Member, IEEE) received the B.E. degree in engineering from Osaka Prefecture University, Sakai, Japan, in 2007, and the M.E. and Ph.D. degrees in engineering from the Tokyo Institute of Technology, Tokyo, Japan, in 2009 and 2012, respectively. In 2010, he was an invited Researcher with Fraunhofer Heinrich Hertz Institute, Berlin, Germany. He is currently an Associate Professor with the Graduate School of Informatics, Kyoto University, Kyoto, Japan. From April 2012 to September 2014, he was a Researcher with the National Institute of Information and Communications Technology (NICT). From October 2014 to December 2021, he was an Assistant Professor with the Graduate School of Informatics, Kyoto University. From January 2021 to September 2022, he was an Associate Professor with the School of Platforms, Kyoto University. His research interests include the topics of physical layer technologies in white space communications, dynamic spectrum access, wireless smart utility networks (Wi-SUN), and 4G/5G/6G systems, including OFDM, OFDMA, MIMO, multi-hop relay network, and full-duplex cellular systems. Since joining NICT, he has been involved in IEEE 802 standardization activities, namely 802.11af, 802.15.4m, and 802.22b. He was the recipient of the Special Technical Awards from IEICE SR technical committee in 2009 and 2017, Best Paper Award from IEICE SR technical committee in 2010 and 2020, Young Researcher's Award from IEICE SRW technical committee in 2016, Best Paper Award from WPMC2017 and WPMC2020, and Best Paper Presentation Award (1st Place) from IEEE WF-IoT 2020.

HIROSHI HARADA (Member, IEEE) is currently a Professor with the Graduate School of Informatics, Kyoto University, Kyoto, Japan, and a Research Executive Director of the Wireless Networks Research Center, National Institute of Information and Communications Technology (NICT). In 1995, he joined the Communications Research Laboratory, Ministry of Posts and Communications (currently, NICT). From 2005 to 2014, he was a Visiting Professor with the University of Electro-Communications, Tokyo, Japan. Since 1995, he has been researched software defined radio, cognitive radio, dynamic spectrum access network, wireless smart ubiquitous network, and broadband wireless access systems on VHF, UHF, microwave, and millimeter-wave bands. In 2014, he was a Professor with Kyoto University. He has also joined many standardization committees and forums in the United States and in Japan and fulfilled important roles for them, especially IEEE 1900 and IEEE 802. He was the Chair of IEEE DySpan Standards Committee and the Vice Chair of IEEE 802.15.4g, IEEE 802.15.4m, 1900.4, and TIA TR-51. He was a board of directors of IEEE communication society standards board, SDR forum, DSA alliance, and WhiteSpace alliance. He is a Co-Founder of Wi-SUN alliance and was the Chairman of the board from 2012 to 2019. He is currently the Vice Chair of IEEE 2857, IEEE 802.15.4aa, and Wi-SUN alliance. He was the Chair of the IEICE Technical Committee on Software Radio and Public Broadband Mobile Communication Development Committee, ARIB. He is also involved in many other activities related to telecommunications. He has authored the book entitled *Simulation and Software Radio for Mobile Communications* (Artech House, 2002). He was the recipient of the achievement awards in 2006 and 2018 and Fellow of IEICE in 2009, respectively and the achievement awards of ARIB in 2009, 2018, and 2022, respectively, on the topic of research and development on cognitive radio and wireless smart utility network.